Agricultural and Forest Meteorology 260–261 (2018) 109–117

Contents lists available at ScienceDirect

Agricultural and Forest Meteorology

journal homepage: www.elsevier.com/locate/agrformet

Multi-model extreme event attribution of the weather conducive to the 2016 Fort McMurray wildfire

Xuezhi Tan[a,b,*], Shu Chen[c], Thian Yew Gan[b]

[a] Department of Water Resources and Environment, Sun Yat-sen University, Guangzhou 510275, PR China
[b] Department of Civil and Environmental Engineering, University of Alberta, Edmonton, Alberta T6G 2W2, Canada
[c] State Key Laboratory of Water Resources and Hydropower Engineering Science, Wuhan University, Wuhan 430072, PR China

ARTICLE INFO

Keywords:
Attribution
Extreme wildfire
Anthropogenic impacts
Climate change
Atmospheric forcings

ABSTRACT

The 2016 Fort McMurray wildfire is the costliest natural disaster in Canadian history attributed to low winter snowpack and extremely warm and dry weather condition in spring. From the perspective of a long-term historical regional climate, we have studied the wildfire weather of the 2016 Fort McMurray, and the role of anthropogenic impacts on the occurrence of such extreme wildfire weather. Twelve model ensembles forced with all forcings, natural forcing, and anthropogenic greenhouse gases forcing, were downscaled and bias-corrected to identify anthropogenic signals in four climate variables and seven wildfire weather indices leading to the occurrence of extreme wildfire weather conditions. Results show large differences in attribution results between twelve models resulting from the inter-model structural uncertainty. However, the role of anthropogenic greenhouse gases emissions in changing the occurrence probability of extremely high temperature is statistically significant, but not on changes in droughts and wildfire weather because of complex moisture changes, concurrent occurrences of extremely high temperature, high wind speed, low precipitation and low relative humidity. The 2016 Fort McMurray wildfire was more likely caused by human-induced warmer spring, whereas anomalously high wildfire weather index values were not likely attributed to anthropogenic impacts. Human activities such as land use change and aerosol emissions could decrease the temperature and precipitation, which are opposite to a warmer and wetter climate expected from the warming effects of rising concentrations of greenhouse gases. Therefore, anthropogenic signals to climate change may be masked when we consider both greenhouse gases emissions and other human activities.

1. Introduction

On May 1, 2016, a wildfire began southwest of Fort McMurray, Alberta, Canada. It swept through the community, forcing the largest wildfire evacuation in the history of Alberta (Kochtubajda et al., 2017). An anomalously dry winter left scanty spring snowpacks which quickly melted under a relatively warm spring. The dry winter and warm spring left plenty of fuel on the ground for wildfires to consume. When the wildfire started, an unusually hot, dry air mass was over northern Alberta, which brought record-breaking temperature ($> 30\,^{\circ}C$) and strong wind (about 72 km/h) to Fort McMurray, which created a perfect condition for an explosive wildfire to occur. As spring snowpack dwindles and disappears earlier under warmer spring temperature because of the effect of global warming, these types of spring fires will likely occur more frequently and with greater severity (Fosu et al., 2016; Westerling et al., 2006; Yoon et al., 2015).

A controversy arose over the debate whether anthropogenic climate change was one of the factors causing the fire, given the role that Fort McMurray plays in Alberta's oil sands industry (Schindler and Donahue, 2006). Given complex interactions between climate, vegetation, fire, and humans, it is challenging to understand how fire activities are affected by changes in climate and human activities on different spatial scales (Pyne, 2001), and to distinguish human and natural impacts on changes to the occurrence of extreme weather conducive to mega-fire events associated with extreme droughts and anomalous warm climate, such as the 2016 Fort McMurray fire. Effects of anthropogenic climate change on the increased forest fire activities (Abatzoglou and Williams, 2016) and droughts (Williams and Abatzoglou, 2016) have been detected in the western United States. Using a single model ensemble, Kirchmeier-Young et al. (2017) detected the anthropogenic forcing to increase the extreme fire risk in entire western Canada. However, the model uncertainty could be substantially larger than the internal variability represented by a single model ensemble (Hawkins and Sutton, 2009), and whether anthropogenic forcings had increased the

* Corresponding author at: Department of Water Resources and Environment, Sun Yat-sen University, Guangzhou 510275, PR China.
E-mail address: tanxuezhi@mail.sysu.edu.cn (X. Tan).

https://doi.org/10.1016/j.agrformet.2018.06.010
Received 7 March 2018; Received in revised form 11 May 2018; Accepted 10 June 2018
Available online 12 June 2018
0168-1923/

occurrence of local extreme weather associated with the 2016 Fort McMurray wildfire remains unclear. Therefore, in this study, we examined whether anomalously warm and dry weather conditions associated with the 2016 extreme wildfire event are attributed to natural climate variability or human-induced climate warming, using a multi-model ensemble to represent the model uncertainty.

Analyses of climate change impacts on Canadian forests often use drought indices which are adequate indicators of fire activities (Girardin et al., 2006). The natural El Niño cycle generally led to a dry fall and winter seasons along with a warm spring over western Canada (Bonsal et al., 2017; Tan et al., 2016; Gan et al., 2007), resulting in a great challenge to separate anthropogenic signals from natural climate variability in the warmer and drier climate. El Niño–Southern Oscillation (ENSO) and Pacific Decadal Oscillation (PDO) modulated the inter-annual to inter-decadal variations of wildfire over western North America. The Atlantic Multidecadal Oscillation could change the spatial and strength of ENSO and PDO influence on the occurrence of wildfire at multi-decadal scales (Kitzberger et al., 2007). El Niño-induced drought also leads to extreme Indonesian fire activity in 2015 (Field et al., 2016), and biomass burning in Indonesia induced by droughts enhanced by human activities (Field et al., 2009). Natural climate variability results in a low signal-to-noise ratio of changes between the occurrence of droughts and wildfire weather.

Other than temperature, drought and wildfire weather involve several other climate variables such as precipitation, wind, and humidity (Zscheischler and Seneviratne, 2017). The dependency between them often lead to weak anthropogenic signals of regional changes in droughts with high temperature and low moisture (Stott et al., 2016), even though anthropogenic signals in increased temperature were widely detected in many regions over western Canada (Gillett et al., 2004) and the world (IPCC, 2013). Even though on the monthly time scale, the temperature could be the best climate variable to predict the area burned (Flannigan and Harrington, 1988), the moisture availability explained the majority of the variance in the annual area burned over Canada in 1959–1999 (Girardin and Wotton, 2009). Thus, anthropogenic signals in temperature change cannot fully represent anthropogenic impacts on changes in the occurrence of droughts or wildfires. For example, Szeto et al. (2016) detected anthropogenic impacts on spring warming but not drying for the 2015 extreme drought in western Canada. However, human influences have quintupled the occurrence probability of extreme vapor pressure deficit for western North America (including western Canada) in 2015/16 (Tett et al., 2017), and human-induced climate change may have increased the risk and severity of the 2015 Alaska fire by 34%–60% (Partain et al., 2016). Kirchmeier-Young et al. (2017) compared fourteen metrics from the Canadian Forest Fire Danger Rating System estimated with large ensembles of the Canadian Earth System Model-2 (CanESM2) between the historical natural forcing (NAT) and the combined natural and anthropogenic forcing (ALL) and found that the effect of anthropogenic forcings have increased the risk of extreme fire events in western Canada by 1.5 to 6 times. The historical NAT forcing mainly includes solar irradiance and volcanic activity while the historical ALL forcing includes the combined effect of natural and anthropogenic forcings such as greenhouse gases, aerosols, ozone, and land-use changes. The response of surface climate to each forcing was investigated by a large ensemble of CanESM2 model simulations. These inconsistent attribution results on anthropogenic signals of changes in droughts (especially moisture or precipitation) over western Canada could result from different climate model simulations, observations and methods. Hauser et al. (2017) presented contradicting conclusions between climate models on anthropogenic signals related to the 2015 European drought using the maximum number of climate models and counterfactual climates with pre-industrial greenhouse gas concentrations.

Given large model uncertainties of anthropogenic signals in changes to regional drought and wildfire weather conditions, in this study, we used a multi-model framework to detect changes in wildfire weather conditions conducive to the 2016 Fort McMurray wildfire and attribute possible climate changes over northern Alberta, Canada to anthropogenic impacts. The remainder of this paper is organized as follows: Section 2 describes the dataset and method used in this analysis; Section 3 presents the analysis results; and Section 4 discusses and concludes the findings.

2. Data and methods

2.1. Observed and GCM data

We collected Canadian historical daily fire weather data from the Canadian Wildland Fire Information System (CWFIS) of the Canadian Forest Service for April 1-October 31, 1971-2016. Together with weather data, we used fuel moisture indices of the Canadian Forest Fire Weather Index system (Van Wagner, 1987) to assess the relative danger of wildfire for the 2016 Fort McMurray wildfire weather condition. The three fuel moisture indices selected are the fine fuel moisture code (ffmc), the duff moisture code (dmc), and the drought code (dc), and four indices representing fire behavior potential, which are fire spread rate (the initial spread index, isi), fuel consumption (the build-up index, bui), fire intensity (the fire weather index, fwi), and daily severity rating (dsr). fwi is an integrated fire danger index based on the other five indices (i.e., ffmc, dmc, dc, isi and bui). Higher fwi values represent higher fire danger potential and vice versa (Wotton, 2009). The above CWFIS indices were calculated from daily noon observed and quality-controlled surface air temperature, 24-h accumulated precipitation, 10-m open wind speed and relative humidity. From the spatial distributions of limited stations and Canadian fire zones (Boulanger et al., 2012), we selected 68 stations near Fort McMurray to represent the regional climate of northern Alberta (120W ~ 110 W and 54N ~ 60 N), which consists of three homogeneous fire regime zones, i.e., Great Slave Lake zone, Southern Prairies zone and Lake Athabasca zone (Fig. 1).

Attribution of the 2016 wildfire event was carried out using ensemble simulations of 12 GCMs (Table 1) selected from the Coupled Model Inter-comparison Project Phase 5 (CMIP5) based on the availability of forcing experiments and input variables to estimate fire weather risks (Taylor et al., 2012). We used simulations driven by the historical ALL forcing, the NAT forcing, and the anthropogenic greenhouse gases (GHG) forcing. The GHG forcing includes only the greenhouse gas forcing and no other anthropogenic forcings such as land use changes, ozone and aerosol emissions. Model simulations under the ALL forcing end in 2005 for all CMIP5 models (Table 1). To fully compare GCM simulations with observations, we extended the historical ALL simulations to 2016 by using projections from the Representative Concentration Pathways 4.5 (RCP4.5) scenario for 2006–2016. Similar extensions were also conducted for previous studies (e.g., Miao et al., 2016; Sun et al., 2014). We focused on the ALL, NAT and GHG simulations of 1950–2016. Some model simulations for NAT and GHG may only end in 2005, so the ensemble mean values of 2006–2016 for these forcings were only obtained from the available model simulations. To provide equal weight to each GCM, we used only one ensemble member for each forcing simulation considered in this study. Four climatic variables over northern Alberta were extracted from GCM outputs for the above three forcings.

2.2. Downscaling and bias-correction of GCM data

We adopted the method used by Kirchmeier-Young et al. (2017) to downscale and bias-correct the multi-model ensemble outputs to the resolution (~ 50 km) of the Modern-Era Retrospective analysis for Research and Applications-2 (MERRA-2; Dirmeyer et al., 2014). Downscaling was done for each climatic variable for each model ensemble by first calculating anomalies on the GCM grid relative to the monthly climatology of that ensemble. These anomalies were then bi-linearly interpolated to a target grid and added by monthly climatology.

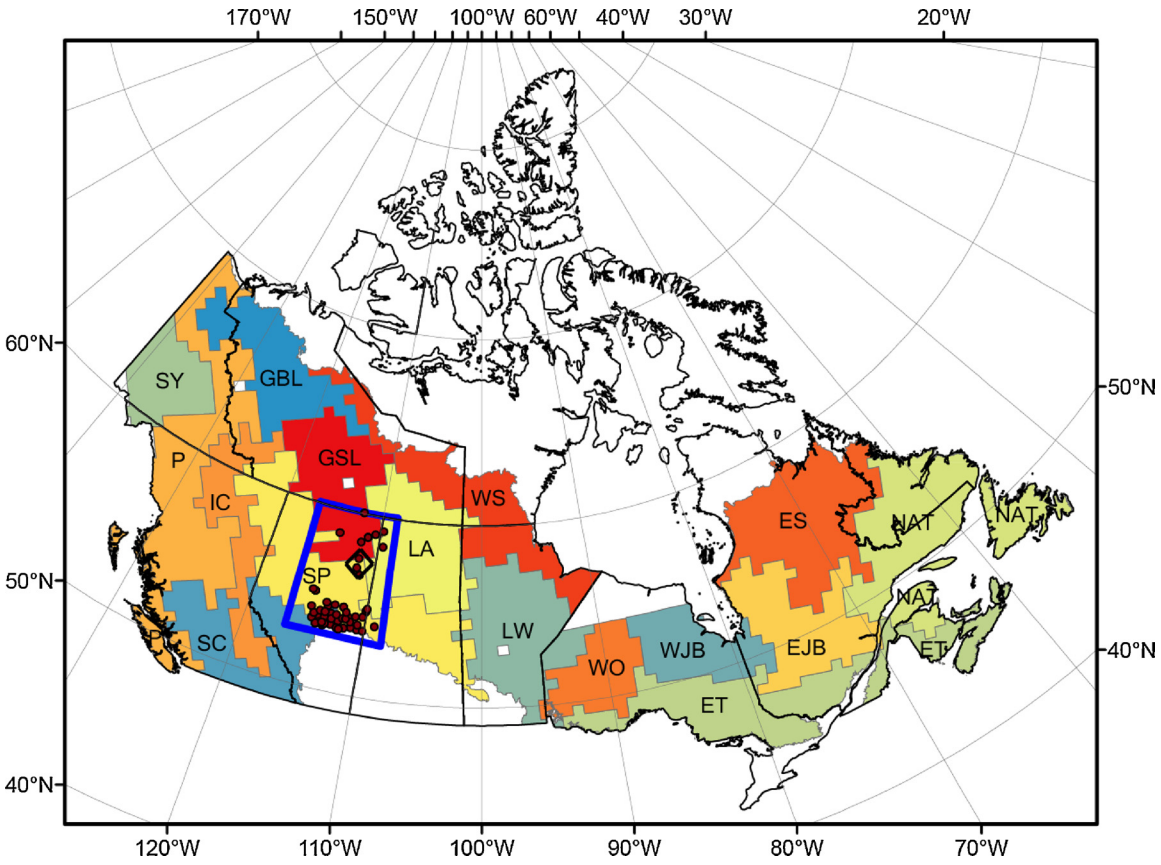

Fig. 1. Map of the study area. The area considered for the wildfire weather analysis is shown in the blue box. The dark red dots show Environment Canada weather stations used in this study. Shadings show the fire zones. SY, Southern Yukon zone; GBL, Great Bear Lake zone; GSL, Great Slave Lake zone; P, Pacific zone; IC, Interior cordillera zone; SC, Southern Cordillera zone; SP, Southern Prairies zone; LA, Lake Athabasca zone; WS, Western Subactic zone, LW, Lake Winnepeg zone; WO, Western Ontario zone; WJB, Western Ontario zone; ET, Eastern temperate zone; EJB, Eastern James Bay zone; ES, Eastern Subarctic zone; NAT, Northern Atlantic zone. Homogeneous fire zones of Canada were reproduced from Boulanger et al. (2012). (For interpretation of the references to colour in this figure legend, the reader is referred to the web version of this article.)

The downscaled climatic variables were then bias-corrected using the multivariate quantile-mapping algorithm of Cannon (2018) which is based on the N-dimensional probability distribution transform (N-pdft) proposed by Pitié et al. (2007). This multivariate bias-correction (MBC) method maintains the multivariate inter-dependence between the four climate variables (temperature, precipitation, relative humidity, and wind speed) and the forced response of the climate model (e.g., changes in quantiles for the four climate variables relative to the ALL baseline). If de-biased separately, the relationship between the four climate variables could be altered, which impacts the calculation of the CWFIS indices (Cannon, 2018). In the original multivariate quantile mapping algorithm (Pitié et al., 2007), the multivariate distribution of the simulations is transformed to match the distribution of observations by iteratively applying a random orthogonal rotation to the datasets followed by univariate quantile mapping of the rotated marginal distributions. The additional rotation step provides linear combinations of the original variables to the univariate quantile mapping bias correction, instead of processing each original variable separately. When the above two sequent steps are repeated and the match eventually converged, the multivariate distribution is corrected. To ensure the bias-corrected GCM simulations preserve the climate change signal of the underlying climate model in the projection period, Cannon (2018) proposed to first apply a change-preserving form of univariate quantile mapping (Cannon et al., 2015) to each variable of the climate model projection dataset and saving the outputs. Next, the multivariate N-pdft algorithm is used to bias-correct both the historical calibration and climate model projection datasets. Finally, the change-preserving quantile mapping outputs in the projection period are reordered according to the ordinal ranks of the corresponding variable from the N-pdft algorithm (Cannon, 2016). Therefore, as described below, the change-preservation property allows the NAT and GHG simulations to maintain their separation from the ALL responses.

In this analysis, we used the MERRA-2 bias-corrected precipitation, and daily maximum temperature, relative humidity, wind-speed, and snow depth as observations to conduct the bias-correction. For each model, the MBC procedure of Cannon (2018) was trained with all available gridded observed data of MERRA-2 for the 1980–2016 baseline period. The ALL, NAT and GHG forcing simulations over the entire period for each model (Table 1) were de-biased using the ALL simulation of that model. The downscaling and bias-correction procedures conducted maintain differences in responses between the ALL, NAT and GHG forcings (Cannon, 2018). The CWFIS indices were then calculated using the downscaled and bias-corrected climate data of ALL, NAT and GHG simulations for each GCM with a common MERRA-2 resolution of ~50 km. Anomalies of the four climatic variables and seven CWFIS indices (three fuel moisture indices and four fire behavior potential indices) for ALL, NAT and GHG forcing ensembles were calculated relative to the climatology of 1960–1990 with the ALL forcing for each GCM.

2.3. Attribution of changes in wildfire weather

We focused on the analysis of regional annual maximum daily anomalies of temperature and wind speed and seven CWFIS indices, and regional annual minimum daily anomalies of precipitation and relative humidity in late spring (April 15th- May 30th) when spring

Table 1
Summary of models used in the analysis.

Modes	Institution	Spatial Resolutions (Latitude × Longitude)	Period of data used for each Forcing			
			ALL	RCP4.5	GHG	NAT
ACCESS1.3	Commonwealth Scientific and Industrial Research Organization (CSIRO) and Bureau of Meteorology (BOM), Australia	1.25 × 1.875	1950-2005	2006-2016	1950-2016	1950-2016
CanESM2	Canadian Center for Climate Modelling and Analysis	2.7906 × 2.8125	1950-2005	2006-2016	1950-2012	1950-2012
CNRM-CM5	Centre National de Recherches Meteorologiques and Centre Europeen de Recherche et Formation Avancees en Calcul Scientifique	1.4008 × 1.40625	1950-2005	2006-2016	1950-2012	1950-2012
CSIRO-Mk3.6.0	Queensland Climate Change Centre of Excellence and Commonwealth Scientific and Industrial Research Organisation	1.8653 × 1.875	1950-2005	2006-2016	1950-2012	1950-2012
GFDL-CM3	NOAA Geophysical Fluid Dynamics Laboratory	2 × 2.5	1950-2005	2006-2016	1950-2005	1950-2005
GFDL-ESM2M	NOAA Geophysical Fluid Dynamics Laboratory	2.0225 × 2.5	1951-2005	2006-2016	1951-2005	1951-2005
HadGEM2-ES	UK Met Office Hadley Centre	1.25 × 1.875	1950-2005	2006-2016	1950-2016	1950-2016
IPSL-CM5A-LR	Institut Pierre Simon Laplace	1.8947 × 3.75	1950-2005	2006-2016	1950-2012	1950-2012
IPSL-CM5A-MR	Institut Pierre Simon Laplace	1.2676 × 2.5	1950-2005	2006-2016	1950-2012	1950-2012
MIROC-ESM	University of Tokyo, National Institute for Environmental Studies, and Japan Agency for Marine-Earth Science and Technology	2.7906 × 2.8125	1950-2005	2006-2016	1850-2005	1850-2005
MIROC-ESM-CHEM	University of Tokyo, National Institute for Environmental Studies, and Japan Agency for Marine-Earth Science and Technology	2.7906 × 2.8125	1950-2005	2006-2016	1850-2005	1850-2005
MRI-CGCM3	Meteorological Research Institute	1.12148 × 1.125	1950-2005	2006-2016	1950-2005	1950-2005

wildfire, e.g., the 2016 Fort McMurray wildfire, would likely occur due to warm and dry weather conditions. For each year and each variable, the value of regional annual maximum (minimum) daily anomaly was the maximum (minimum) daily value of that variable in all grid cells of downscaled GCM simulations (~50 km resolution), or the observed daily values in all stations in that day. We define an extreme event as a particular climate variable or a CWFIS index exceeding a chosen threshold. Regional maximum MERRA-2 values over the northern Alberta during April 15th- May 30th when the Fort McMurray wildfire occurred are thresholds for detecting anthropogenic impacts on the occurrence of the 2016 Fort McMurray wildfire. We also considered a wide rage of thresholds to see possible differences of anthropogenic impacts to different extreme wildfire risk with various wildfire weather conditions. We estimated the conventional fraction of attributable risk ($FAR = 1 - P_{NAT}/P_{ALL}$ and $FAR_{GHG} = 1 - P_{NAT}/P_{GHG}$) (Stone and Allen, 2005; Stott, 2015) to estimate changes in risk attributable to an external forcing. P_{ALL}, P_{NAT}, and P_{GHG} are the occurrence probability of the extreme wildfire under the historical ALL, NAT and GHG forcings, respectively. Differences in the probability of extreme spring fire weather anomalies between the ALL or GHG forcing (P_{ALL} or P_{GHG}) and NAT forcing (P_{NAT}) simulations show anthropogenic or greenhouse gases emissions contributed to changes in the occurrence of extreme wildfire events such as the observed 2016 Fort McMurray. We also estimated the risk ratio ($RR = P_{ALL}/P_{NAT}$ and $RR_{GHG} = P_{GHG}/P_{NAT}$) that shows how many times the probability of occurrence of an event for ALL/GHG than for NAT. Since we found significant differences in reproducing the wildfire weather between GCMs (Figs. 2 and 3), we respectively estimated *FAR* and *RR* for each model ensemble which has been downscaled and bias-corrected, instead of using multi-model ensemble mean responses to different forcings. For each model, we calculated the P_{ALL}, P_{NAT} and P_{GHG} based on the density (Fig. 3) of daily time series of anomalies for each variable during April 15th- May 30th in 1950-2016. The uncertainty of *FAR* and *RR* for each model ensemble was estimated by the bootstrapping method, and the inter-model uncertainty of *FAR* and *RR* was the combined uncertainty range of *FAR* and *RR* for all models.

3. Results

Fig. 2 shows the time series of regional annual maximum anomalies of temperature, wind speed, bui, and fwi, and regional annual minimum anomalies of precipitation, relative humidity over the study region (northern Alberta), while Fig. 3 shows the density distribution functions for regional maximum daily anomalies of the three forcings and station observed climate variables. Because large variabilities were often averaged out in the gridded data, station data generally show more extreme values than downscaled and bias-corrected GCMs' simulations. Furthermore, the equal-weighting of the stations would likely not be representative of the region of interest, given the large clump of stations in the southern portion. The extreme wildfire weather condition for the 2016 Fort McMurray wildfire was caused by the anomalously high temperature (Fig. 2a) and low relative humidity (Fig. 2c). The 2016 Fort McMurray was less serious than the 1981 spring wildfire over northern Alberta (Harvey and Alexander, 1986) which resulted from anomalously high temperature (Fig. 2b) and low precipitation (Fig. 2d). Total area burned in Alberta during 1981 was concurrent with extremely high values of fire behavior potential indices, e.g., bui and fwi (Fig. 2e-f). The probability density distributions of climate and wildfire weather variables between ALL forcing and station observations cannot be directly compared. However, regional annual extreme anomalies in the station data show the observed changes in the wildfire weather over northern Alberta. Trends in observed temperature (Fig. 2a), relative humidity (Fig. 2c) and bui (Fig. 2e) anomalies generally agree with trends of multi-ensemble mean simulations of 12 GCMs of CMIP5 under the ALL forcing, but trends in observed precipitation (Fig. 2b), wind speed (Fig. 2d) and fwi (Fig. 2f)

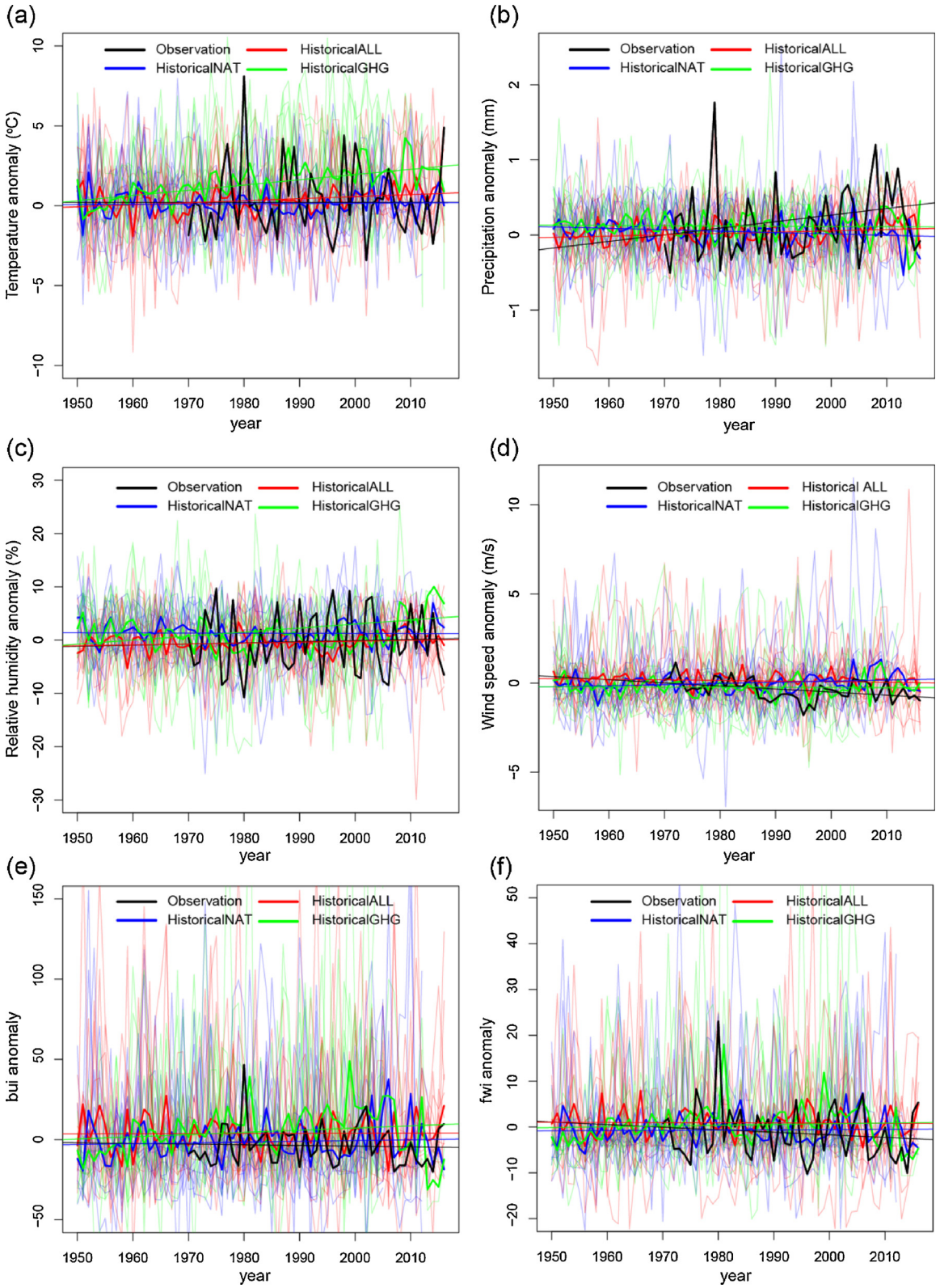

Fig. 2. Time series of annual maximum values of regional maximum/minimum anomaly on April 15th- May 30th of temperature (a), precipitation (b), relative humidity (c), wind speed (d), fire buildup index (bui; e), and fire weather index (fwi; f) for station observations in black, ALL forcing (HistoricalALL) ensemble mean in red, NAT forcing (HistoricalNAT) in blue, and GHG (HistoricalGHG) forcing in green. Colorful bold lines show multi-model ensemble mean values for each forcing. The straight lines show the trends of each variable with the color corresponding to that forcing. Anomalies for ALL, NAT and GHG forcing ensembles are calculated relative to the ALL ensemble mean climatology in 1960–1990 for each model. (For interpretation of the references to colour in this figure legend, the reader is referred to the web version of this article.)

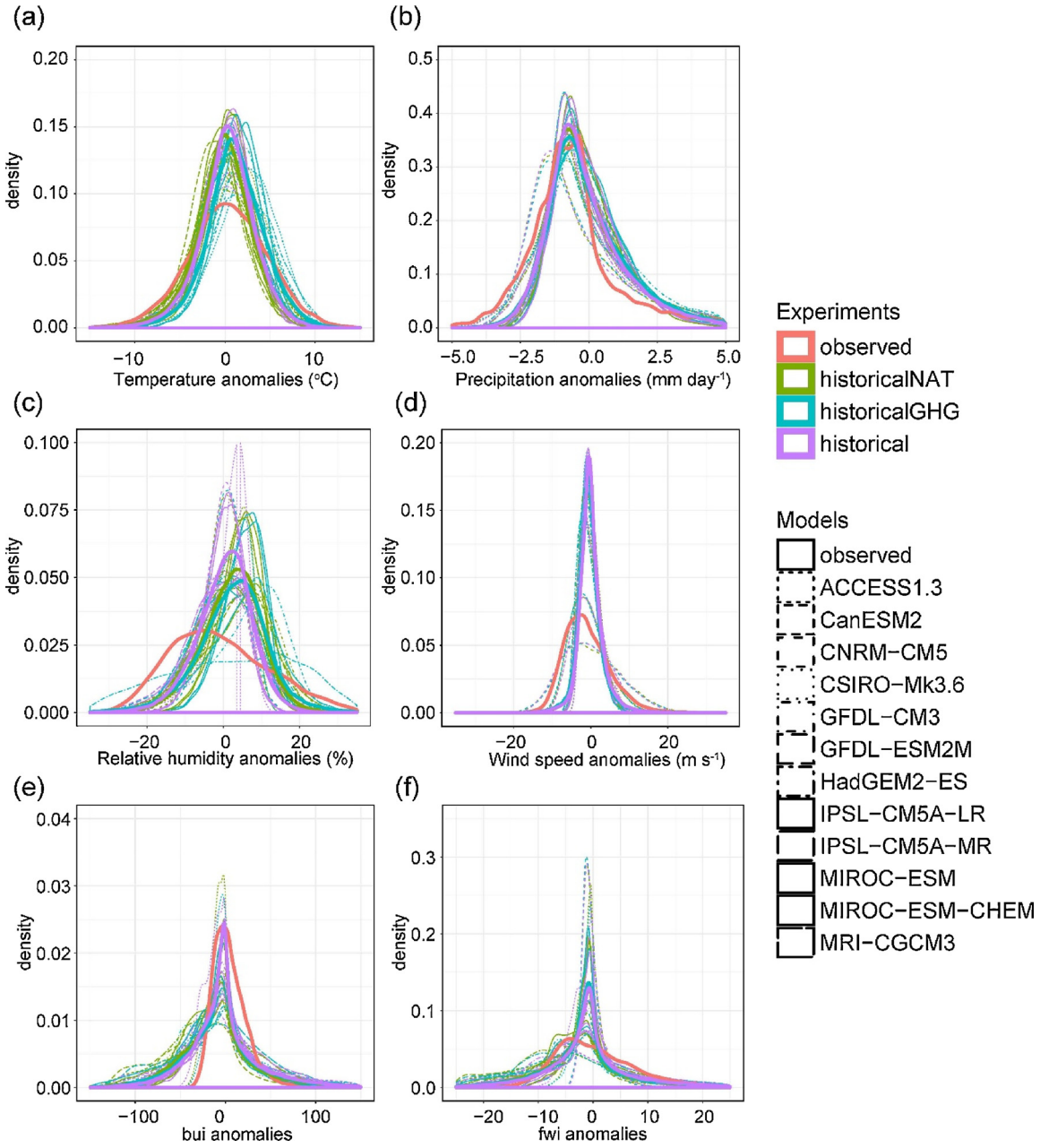

Fig. 3. Density plots for ensemble regional maximum values of daily temperature (a), precipitation (b), relative humidity (c), wind speed (d), fire buildup index (bui; e), and fire weather index (fwi; f) for station observations, ALL forcing (HistoricalALL), NAT forcing (HistoricalNAT), and GHG (HistoricalGHG) forcing. Shaded lines show regional mean values for each ensemble. Ensemble mean values are pooled from the ensemble members and probability distributions are estimated by a Gaussian kernel density estimator.

anomalies differ from those of the multi-ensemble mean simulations of the 12 GCMs under the ALL forcing.

Even though there are large differences between anomalies of different climate models, both bui and fwi show that weather with higher wildfire risks dominates climate model simulations under ALL and GHG forcing compared to climate model simulations under NAT forcing (Figs. 2 and 3), even though precipitation simulated under ALL and GHG forcings is generally higher than under NAT forcing. Relative humidity simulated under ALL forcing are lower than those under the NAT forcing because of higher temperature simulated by ALL forcing, giving rise to higher moisture holding capacity, compared to NAT forcing. This is not surprising according to the Clausius–Clapeyron relationship, as the saturation vapor pressure will increase by about 7% for every K rise in temperature (Boer, 1993). Therefore, as the climate warms, a warmer atmosphere will have a larger capacity to hold more water vapor. Thus the relative humidity would become low given the moisture supply is constant. However, wildfire weather indices (bui and fwi) in ALL forcing do not increase as fast as temperature because of a slight increase in precipitation but a decrease in wind speed. This contrasting projected increase or decrease in the four fire-related climate variables lead to projected complex changes in wildfire weather. The projected increase (decrease) in the regional maximum GHG bui (observed fwi) is statistically significant ($p = 0.01$) according to the Mann Kendall test, while bui and fwi projected under other forcings do not show statistically significant changes.

Fig. 4 shows the *RR* for anomalies of climate variables and wildfire weather indices on different threshold values. Due to large differences between climate models in the attribution results, there is a large uncertainty of the *RR* for all variables (except temperature in the GHG forcing), especially for extremely high threshold values. Therefore, it is

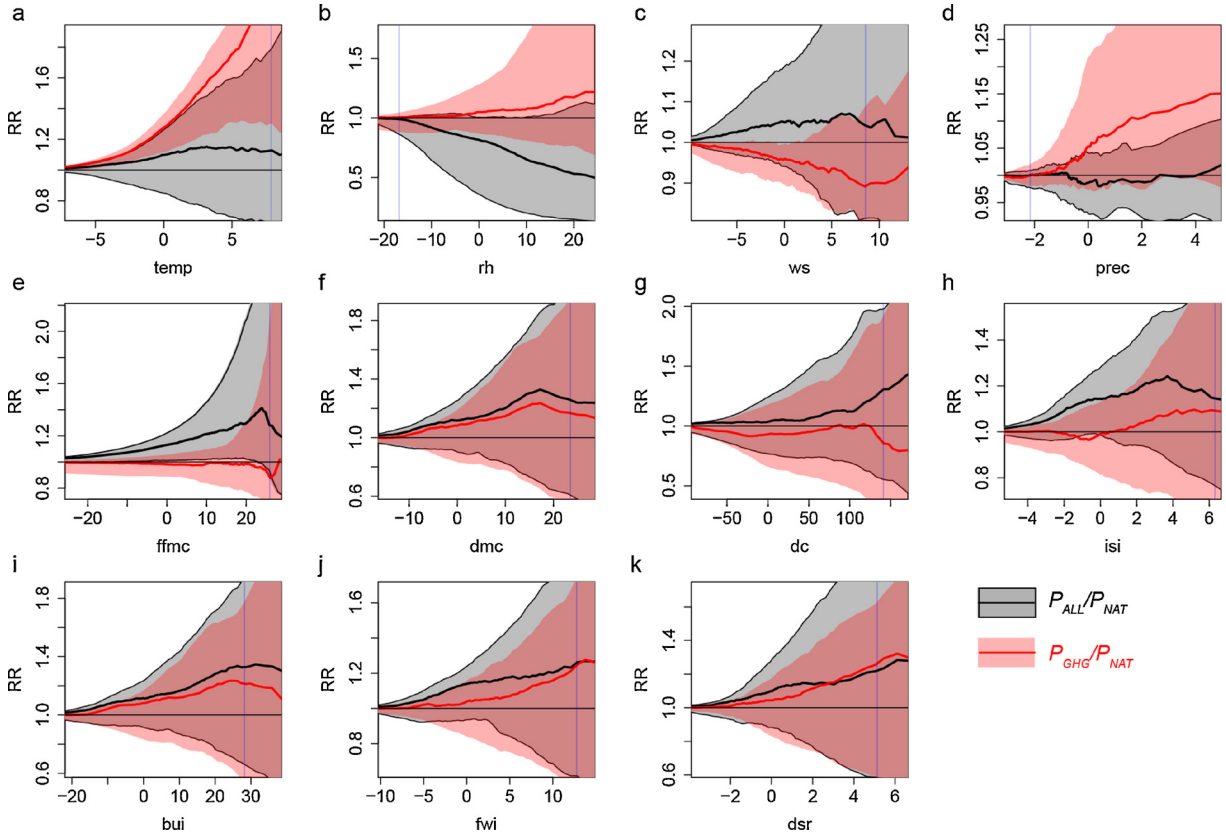

Fig. 4. The risk ratio (RR) for anomalies of climate variables (a, temperature; b, relative humidity; c, wind speed; and d, precipitation) and wildfire weather indices (e, ffmc; f, dmc; g, dc; h, isi; i, bui; *j*, fwi; and k, dsr) based on a 1960–1990 climate. For an event more extreme than values indicated on the horizontal axis, the RR shows the probability ratio of that event occurrence under ALL forcing (black line and shade area) or GHG forcing (red line and shade area) to NAT forcing. The shaded area shows the uncertainty range (5–95%) for each RR curve of 12 GCM simulations. The vertical shaded blue lines show regional maximum (minimum) daily anomalies of temperature and wind speed and seven FWI system indices (precipitation and humidity) on April 15th- May 30th, 2016 when the 2016 Fort McMurray wildfire occurred. (For interpretation of the references to colour in this figure legend, the reader is referred to the web version of this article.)

unclear whether the occurrence of extreme weather conducive to 2016 Fort McMurray wildfire can be attributed to anthropogenic activities. However, there are differences between *RR* of ALL and GHG forcings, which demonstrate that besides greenhouse gases emissions, anthropogenic activities such as land use change, ozone and aerosol emissions could have contributed to climate change impacts.

For temperature, *RR* values for the threshold value of the 2016 Fort McMurray are 0.7–1.7 (1.2–3.8) times more likely, with an average of 1.1 (1.7) under ALL (GHG) forcing (Fig. 4a), which corresponds to 10% (40%) of the risk for the extremely high temperature of the 2016 Fort McMurray to be attributed to anthropogenic (increased greenhouse emissions) impacts on climate change, i.e., *FAR* = 10% (40%) (Fig. 5a). However, extremely low precipitation leading to the 2016 Fort McMurray wildfire could not be attributed to either ALL or GHG forcings, as GHG forcing results in increased precipitation while compared to NAT forcing, and ALL forcing does not contribute to changes in precipitation over northern Alberta. Differences in both the response of temperature and precipitation to GHG and ALL forcings may demonstrate the sensitivity of climate to aerosol cooling on regional scales (Salzmann, 2016). Non-significant *RR* values for relative humidity and wind speed are also found for GHG and ALL forcings which demonstrate that we cannot attribute the 2016 Fort McMurray wildfire to human-induced drier spring (Fig. 4b and 4c), as relative humidity and wind speed are highly associated with evaporation.

As expected, for CWFIS indices (Fig. 4e-k), *RR* values increase as the climate becomes riskier to occurrences of wildfire, which means that the possibilities of anthropogenic impacts leading to weather conducive to the occurrence of wildfire increase under high CWFIS indices. Statistically significant anthropogenic signals of ffmc are detected in ALL forcing, as *RRs* for ffmc anomalies < 20 are generally larger than 1. About 20% of the risk (*FAR* ≈ 10%) for getting extremely high bui and fwi values could be attributed to anthropogenic forcings. However, inter-model differences in *RR* are also large for both GHG and ALL forcings, partly because of uncertainties associated with simulations of CMIP5 GCMs. The multi-model ensemble mean *RR* values (~1.4) are substantially lower than those (1.5–6) derived for western Canada using only the CanESM2 model ensembles (Kirchmeier-Young et al., 2017). Note that it is not directly comparable our *RR* results to those of Kirchmeier-Young et al. (2017) because they studied the entire fire season over western Canada while we focus on the spring and northern Alberta. Event attribution results can be sensitive to the framing of the attribution question (National Academies of Sciences, Engineering, and Medicine, 2016). Here we just discuss differences in the uncertainty ranges. The range of *RR* results derived from CanESM2 for our study is 1.8-2.2. As expected, the inter-model variance we obtained which shows model structural uncertainty is substantially higher than the intra-model variance obtained by Kirchmeier-Young et al. (2017) which only shows natural internal variability.

4. Discussion and conclusions

Large differences in attribution results between climate models and non-significant anthropogenic signals detected from the multi-model attribution study for the 2016 Fort McMurray wildfire show that multi-model ensembles are necessary to adequately represent the structural uncertainty of the climatic simulations for climate detection and attribution analyses. We used the MBC method to de-bias the downscaled GCM simulations for all twelve climate models relative to the MERRA-2

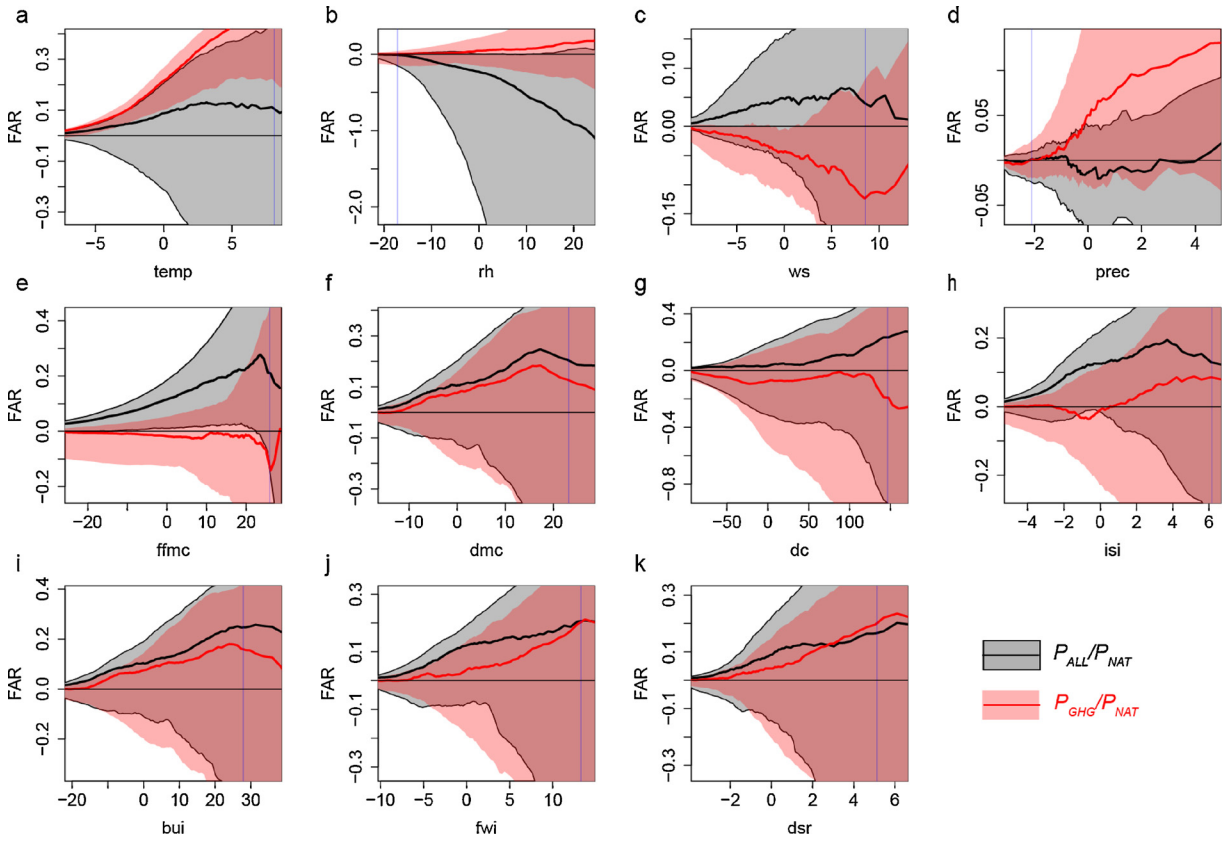

Fig. 5. Same as Fig. 4, but for FAR.

reanalysis, even though at times the downscaling and bias-correction processes may introduce additional sources of uncertainty or errors (Maraun et al., 2017). The effectiveness of bias-correction of climate variables simulated by climate models based on the MERRA-2 reanalysis data for the study site depends on the accuracy of the reanalysis data and the multivariate quantile-mapping algorithm used.

The wide range of *FAR*s and *RR*s obtained in this study imply that multi-climate models do not consistently simulate the variability and changes in extreme wildfire weather over northern Alberta under different forcings. Even though the role of anthropogenic greenhouse gases emissions in changing the occurrence probability of extremely high temperature is statistically significant, anthropogenic impacts on changes in droughts and wildfire weather remain uncertain, partly because of inconsistent projected changes in moisture and the concurrent occurrence of extremely high temperature and wind speed while low precipitation and relative humidity. As anthropogenic signals in a single climate variable (e.g., temperature or precipitation) are more discernable than those of wildfire weather indices which involves multiple climate variables, multivariate hydroclimatic frequency analysis is proposed to identify changes in the dependency between multiple variables for multi-model ensembles (e.g., Zscheischler and Seneviratne, 2017).

Human activities such as land use change and aerosol emissions could decrease temperature and precipitation, which are opposite to a warmer and wetter climate resulting from rising concentration of greenhouse gases. Therefore, anthropogenic signals to climate change may be masked when we consider both greenhouse gases emissions and other human activities (ALL). Despite small differences in regional climate responses simulated under ALL and NAT forcings over northern Alberta, GHG forcing increases occurrence frequency of extremely high temperature and precipitation. The 2016 Fort McMurray wildfire was more likely caused by anthropogenic impacts to the warmer spring. Szeto et al. (2016) also attributed to the 2015 extreme drought in western Canada to anthropogenic impacts to warm spring, instead of human-induced dry weather condition. In contrast to climate variables that responded to ALL and GHG forcings differently, the majority of wildfire indices (except ffmc) show similar responses to ALL and GHG forcing. This shows the insensitivity of wildfire indices to the projected climate change under different forcings.

Acknowledgments

The first author was partly funded by the China Scholarship Council (CSC) of P.R. China, and the University of Alberta. We are grateful to Bo Lu from the Canadian Forest Service (http://cwfis.cfs.nrcan.gc.ca/ha/nfdb) for providing the station observed climate and wildfire weather data. The R package “MBC” for bias-correction based on the multivariate quantile-mapping algorithm is provided by Alex *J*. Cannon https://cran.r-project.org/web/packages/MBC/. We thank the World Climate Research Programme’s Working Group on Coupled Modelling for producing and making available their model output. Thank two anonymous reviewers for their constructive comments and suggestions which greatly help us improve the manuscript significantly.

References

Abatzoglou, J.T., Williams, A.P., 2016. Impact of anthropogenic climate change on wildfire across western US forests. Proc. Natl. Acad. Sci. U. S. A. 113 (42), 11770–11775. http://dx.doi.org/10.1073/pnas.1607171113.

Boer, G.J., 1993. Climate change and the regulation of the surface moisture and energy budgets. Clim. Dynam. 8, 225–239. http://dx.doi.org/10.1007/BF00198617.

Bonsal, B.R., Cuell, C., Wheaton, E., Sauchyn, D.J., Barrow, E., 2017. An assessment of historical and projected future hydro-climatic variability and extremes over southern watersheds in the Canadian Prairies. Int. J. Climatol. 37 (10), 3934–3948. http://dx.doi.org/10.1002/joc.4967.

Boulanger, Y., Gauthier, S., Burton, P.J., Vaillancourt, M.-A., 2012. An alternative fire regime zonation for Canada. Int. J. Wildland Fire 21 (8), 1052–1064. http://dx.doi.org/10.1071/wf11073.

Cannon, A.J., 2016. Multivariate bias correction of climate model outputs: matching

marginal distributions and inter-variable dependence structure. J. Clim. 29 (19), 7045–7064.
Cannon, A.J., 2018. Multivariate quantile mapping bias correction: an n-dimensional probability density function transform for climate model simulations of multiple variables. Clim. Dynam. 50, 31–49. http://dx.doi.org/10.1007/s00382-017-3580-6.
Cannon, A.J., Sobie, S.R., Murdock, T.Q., 2015. Bias correction of GCM precipitation by quantile mapping: how well do methods preserve changes in quantiles and extremes? J. Clim. 28 (17), 6938–6959.
Dirmeyer, P.A., Wei, J., Bosilovich, M.G., Mocko, D.M., 2014. Comparing evaporative sources of terrestrial precipitation and their extremes in MERRA using relative entropy. J. Hydrometeorol. 15 (1), 102–116. http://dx.doi.org/10.1175/jhm-d-13-053.1.
Field, R.D., van der Werf, G.R., Shen, S.S.P., 2009. Human amplification of drought-induced biomass burning in Indonesia since 1960. Nat. Geosci. 2 (3), 185–188. http://dx.doi.org/10.1038/ngeo443.
Field, R.D., et al., 2016. Indonesian fire activity and smoke pollution in 2015 show persistent nonlinear sensitivity to El nino-induced drought. Proc. Natl. Acad. Sci. U. S. A. 113 (33), 9204–9209. http://dx.doi.org/10.1073/pnas.1524888113.
Flannigan, M.D., Harrington, J.B., 1988. A study of the relation of meteorological variables to monthly provincial area burned by wildfire in Canada (1953-80). J. Appl. Meteorol. Clim. 27 (4), 441–452.
Fosu, B.O., Wang, S.-Y.S., Yoon, J.-H., 2016. The 2014/15 snowpack drought in washington state and its climate forcing. Bull. Am. Meteorol. Soc. 97 (12), S19–S24. http://dx.doi.org/10.1175/BAMS-D-16-0154.1.
Gan, T.Y., Gobena, A., Wang, Q., 2007. Precipitation of southwestern Canada: wavelet, scaling, multifractal analysis, and teleconnection to climate anomalies. J. Geophys. Res.–Atm. 112http://dx.doi.org/10.1029/2006jd007157. D10110.
Gillett, N.P., Weaver, A.J., Zwiers, F.W., Flannigan, M.D., 2004. Detecting the effect of climate change on Canadian forest fires. Geophys. Res. Lett. 31http://dx.doi.org/10.1029/2004GL020876. L18211.
Girardin, M.P., Wotton, B.M., 2009. Summer moisture and wildfire risks across Canada. J. Appl. Meteorol. Clim. 48 (3), 517–533. http://dx.doi.org/10.1175/2008jamc1996.1.
Girardin, M.P., Tardif, J.C., Flannigan, M.D., Bergeron, Y., 2006. Forest fire-conducive drought variability in the Southern Canadian boreal forest and associated climatology inferred from tree rings. Can. Water Resour. J. 31 (4), 275–296. http://dx.doi.org/10.4296/cwrj3104275.
Hauser, M., Gudmundsson, L., Orth, R., Jézéquel, A., Haustein, K., Vautard, R., van Oldenborgh, G.J., Wilcox, L., Seneviratne, S.I., 2017. Methods and model dependency of extreme event attribution: the 2015 European drought. Earth' Future 5 (10), 1034–1043. http://dx.doi.org/10.1002/2017ef000612.
Hawkins, E., Sutton, R., 2009. The potential to narrow uncertainty in regional climate predictions. Bull. Amer. Meteorol. Soc. 90 (8), 1095–1107.
IPCC, 2013. In: Stocker, T.F., Qin, D., Plattner, G.-K., Tignor, M., Allen, S.K., Boschung, J., Nauels, A., Xia, Y., Bex, V., Midgley, P.M. (Eds.), Climate Change 2013: The Physical Science Basis. Contribution of Working Group I to the Fifth Assessment Report of the Intergovernmental Panel on Climate Change. Cambridge University Press, Cambridge, United Kingdom and New York, NY, USA 1535 pp.
Kirchmeier-Young, M.C., Zwiers, F.W., Gillett, N.P., Cannon, A.J., 2017. Attributing extreme fire risk in Western Canada to human emissions. Clim. Change 144 (2), 365–379. http://dx.doi.org/10.1007/s10584-017-2030-0.
Kitzberger, T., Brown, P.M., Heyerdahl, E.K., Swetnam, T.W., Veblen, T.T., 2007. Contingent pacific-Atlantic Ocean influence on multicentury wildfire synchrony over western North America. Proc. Natl. Acad. Sci. U. S. A. 104 (2), 543–548. http://dx.doi.org/10.1073/pnas.0606078104.
Kochtubajda, B., Brimelow, J., Flannigan, M., Morrow, B., Greenhough, M.D., 2017. The extreme 2016 wildfire in Fort mcmurray, Alberta, Canada. In "State of the climate in 2016". Bull. Am. Meteorol. Soc. 98 (8), S176–S177.
Maraun, D., et al., 2017. Towards process-informed bias correction of climate change simulations. Nat. Clim. Change 7 (11), 664–773. http://dx.doi.org/10.1038/nclimate3418.
Miao, C., Sun, Q., Kong, D., Duan, Q., 2016. Record-breaking heat in northwest China in July 2015: analysis of the severity and underlying causes. Bull. Am. Meteorol. Soc. 97 (12), S97–S101.
National Academies of Sciences, Engineering, and Medicine, 2016. Attribution of Extreme Weather Events in the Context of Climate Change. The National Academies Press, Washington, DC.
Partain, J.L., et al., 2016. An assessment of the role of anthropogenic climate change in the Alaska fire season of 2015. Bull. Am. Meteorol. Soc. 97 (12), S14–S18.
Pitié, F., Kokaram, A.C., Dahyot, R., 2007. Automated colour grading using colour distribution transfer. Comput. Vis. Image Underst. 107 (1-2), 123–137.
Pyne, S.J., 2001. The fires this time, and next. Science 294 (5544), 1005–1006. http://dx.doi.org/10.1126/science.1064989.
Salzmann, M., 2016. Global warming without global mean precipitation increase. Sci. Adv. 2http://dx.doi.org/10.1126/sciadv.1501572. e1501572.
Schindler, D.W., Donahue, W.F., 2006. An impending water crisis in Canada's western prairie provinces. Proc. Natl. Acad. Sci. U. S. A. 103 (19), 7210–7216. http://dx.doi.org/10.1073/pnas.0601568103.
Stone, D.A., Allen, M.R., 2005. The end-to-end attribution problem: from emissions to impacts. Clim. Change 71 (3), 303–318. http://dx.doi.org/10.1007/s10584-005-6778-2.
Stott, P., 2015. Attribution: weather risks in a warming world. Nat. Clim. Change 5 (6), 517–518. http://dx.doi.org/10.1038/nclimate2640.
Stott, P.A., et al., 2016. Attribution of extreme weather and climate-related events. Wiley Interdiscip. Rev. Clim. Change 7 (1), 23–41. http://dx.doi.org/10.1002/wcc.380.
Sun, Y., Zhang, X., Zwiers, F.W., Song, L., Wan, H., Hu, T., Yin, H., Ren, G., 2014. Rapid increase in the risk of extreme summer heat in Eastern China. Nat. Clim. Change 4, 1082–1085. http://dx.doi.org/10.1038/nclimate2410.
Szeto, K., Zhang, X., White, R.E., Brimelow, J., 2016. The 2015 extreme drought in western Canada. Bull. Amer. Meteor. Soc. 97 (12), S42–S46. http://dx.doi.org/10.1175/BAMS-D-16-0149.
Tan, X., Gan, T.Y., Shao, D., 2016. Wavelet analysis of precipitation extremes over Canadian ecoregions and teleconnections to large-scale climate anomalies. J. Geophys. Res. Atmos. 121 (24), 14469–14486. http://dx.doi.org/10.1002/2016jd025533.
Taylor, K.E., Stouffer, R.J., Meehl, G.A., 2012. An overview of CMIP5 and the experiment design. Bull. Amer. Meteor. Soc. 93 (4), 485–498. http://dx.doi.org/10.1175/BAMS-D-11-00094.1.
Tett, S.F.B., et al., 2017. Anthropogenic forcings and associated changes in fire risk in western north america and australia during 2015/16. Bull. Am. Meteorol. Soc. 98 (12), S60–S63. http://dx.doi.org/10.1175/BAMS-D-17-0096.1.
Van Wagner, C.E., 1987. Development and Structure of the Canadian Forest Fire Weather index System. Forestry Technical Report 35Rep. Canadian Forest Service, Ottawa.
Westerling, A.L., Hidalgo, H.G., Cayan, D.R., Swetnam, T.W., 2006. Warming and earlier spring increase western US forest wildfire activity. Science 313 (5789), 940–943.
Williams, A.P., Abatzoglou, J.T., 2016. Recent advances and remaining uncertainties in resolving past and future climate effects on global fire activity. Curr. Climate Change Reports 2 (1), 1–14. http://dx.doi.org/10.1007/s40641-016-0031-0.
Wotton, B.M., 2009. Interpreting and using outputs from the Canadian Forest fire danger rating system in research applications. Environ. Ecol. Stat. 16 (2), 107–131. http://dx.doi.org/10.1007/s10651-007-0084-2.
Yoon, J.-H., Wang, S.-Y.S., Gillies, R.R., Hipps, Le., Kravitz, B., Rasch, P.J., 2015. Extreme fire season in california: a glimpse into the future? Bull. Am. Meteorol. Soc. 96 (12), S5–S9. http://dx.doi.org/10.1175/BAMS-D-15-00114.1.
Zscheischler, J., Seneviratne, S.I., 2017. Dependence of drivers affects risks associated with compound events. Sci. Adv. 3 (6). http://dx.doi.org/10.1126/sciadv.1700263. e1700263.